East European Journal of Physics. 4. 308-318 (2025)
DOI:10.26565/2312-4334-2025-4-29 ISSN 2312-4334

THREE-DIMENSIONAL MHD FLOW AND HEAT TRANSFER OF WATER-BASED NANOFLUIDS OVER A STRETCHING SURFACE WITH CORIOLIS FORCE AND THERMAL EFFECTS

M.M. Bindu[1,2], Elliriki Mamatha[2], V. Nagaradhika[3]*
[1]*Government first grade college, Channapatna, 562160, India*
[2]*Department of Mathematics, GSS, GITAM Deemed to be University, Benguluru-561203, India*
[3]*Department of Mathematics, Sir M. Visvesvaraya Institute of Technology, Bengaluru -562 157, India*
**Corresponding Author E-mail: nagaradhika79@gmail.com*
Received July 9, 2025; revised September 9, 2025; accepted September 12, 2025

This study focuses on the thermal behavior and three-dimensional boundary layer flow of water-based nanofluids over a stretched surface, considering the combined effects of Coriolis and Lorentz forces. The model includes several important physical aspects such as surface convection, internal heat generation, Joule heating, viscous dissipation, and thermal radiation. Copper (Cu), aluminum oxide (Al_2O_3), and magnetite (Fe_3O_4) nanoparticles are dispersed in water to compare their effectiveness in enhancing heat transfer. By applying similarity transformations, the complex system of partial differential equations is reduced to a set of nonlinear ordinary differential equations, which are then solved numerically using the Runge-Kutta-Fehlberg method along with the shooting technique. The results show that nanofluids containing Cu nanoparticles provide the highest thermal performance, followed by those with Al_2O_3 and Fe_3O_4. These findings highlight the importance of selecting appropriate nanoparticles to improve heat transfer efficiency in thermal management applications. Increasing rotation parameter λ suppresses the axial velocity while simultaneously reducing the temperature distribution, highlighting the damping influence of rotational effects on momentum and heat transport.
Keywords: *Nonlinear thermal radiation; Nanofluid; Rotational Effects; Viscous dissipation; Joule heating*
PACS: 44.30.+v, 44.05.+e, 66.10.cd, 47.11.-j

INTRODUCTION

The integration of nanoparticles into traditional base fluids has opened new avenues in the domain of heat transfer enhancement. Nanofluids are highly developed fluids that have the potential to revolutionize several industrial processes. Their exceptional thermal conductivity and energy transfer characteristics make them ideal for electronic cooling, heat exchangers, and automotive systems, among many other uses. The foundational concept was introduced by Choi and Eastman [1], who demonstrated that suspending nanoparticles within a fluid significantly enhances its thermal performance. Subsequently, Buongiorno [2] arrived to the conclusion that the incorporation of nanoparticles causes an abnormal rise in the host fluid's thermal conductivity by presenting a theoretical framework that incorporates many slip processes to simulate nanofluid behavior.

A number of scholars have built upon this base via numerical and experimental investigations. As an example, Wang et al. [3] Sheikholeslami and Rokni studied vegetable oil nanofluid lubrication. [4] nanofluid flow was investigated in relation to magnetic fields. Khan and Pop [5] Computational techniques were used to study nanofluid boundary layer flow across a stretched surface. Krishnamurthy et al. also excelled. [6], who analyzed heat transfer in nanofluids over exponentially stretching surfaces, and Muqaddass et al. [7], Considering hybrid nanofluids under time-dependent thermal and external magnetic fields. Researchers like Nadeem et al. [8], Asadi et al. [9], and Das et al. [10] have also shed light on hybrid nanofluids, stability, and computational methods for difficult flow issues. Laila [11] investigated nanofluid flow in converging and diverging channels with rectangular and heated walls, demonstrating the strong influence of wall geometry on the velocity and temperature fields. Extending this line of research, Rehman et al. [12] examined nanofluid flow over an inclined cylindrical surface in a double-stratified medium. Complementarily, Makinde [13] developed computational models for nanofluid flow over a convectively heated unsteady stretching sheet, emphasizing the importance of transient effects and convective boundary conditions in thermal performance. Recent studies have also incorporated magnetic and hybrid nanofluid effects. Akbar et al. [14] analyzed magnetized Casson hybrid nanofluid flow in a converging-diverging channel with radiative heat transfer. Similarly, Khan et al. [15] investigated mixed convection hybrid nanofluid flow over a permeable, moving, and inclined flat plate, where thermophoresis and radiative heat flux were found to influence both momentum and energy transport significantly. Gireesha and Anitha [16] studied convective flow through a permeable microchannel, with irreversibility analysis demonstrating the thermodynamic implications of such fluids. Madhukesh et al. [17] introduced the concept of pollutant dispersion into nanofluid flows across a stretched disc-cone device, establishing the interplay between nanoparticle transport and environmental effects. Furthermore, Cheng et al. [18] performed nonsimilar forced convection simulations of water-copper nanofluid through a porous medium, considering thermal radiation, heat generation, and viscous dissipation, which added further realism to nanofluid modeling in porous environments. Sheikholeslami and Shehzad [19] studied magnetohydrodynamic (MHD) nanofluid

Cite as: M.M. Bindu, E. Mamatha, V. Nagaradhika, East Eur. J. Phys. 4, 308 (2025), https://doi.org/10.26565/2312-4334-2025-4-29

convection in a porous enclosure with heat flux boundary conditions, showing how porous media significantly alter convection patterns under magnetic influence. Jyoti et al. [20] analyzed kerosene-alumina nanofluid flow between parallel plates with nonlinear convection and radiative heat transfer, incorporating variable viscosity to highlight the sensitivity of transport processes to temperature-dependent properties.

The Coriolis force plays a pivotal role in rotating fluid systems and is relevant in geophysical, industrial, and mechanical contexts, such as rotating machinery, centrifuges, viscometers, and disk drives. The classic analysis of rotating flows began with the work of Kármán [21], who formulated similarity transformations for the rotating disk problem. This foundation was extended by Wang [22] and further advanced by Nazar et al. [23] through the application of numerical techniques. To ensure the reliability of the present analysis, our results have been compared with the findings reported in these studies, and an excellent level of agreement has been observed, thereby validating the accuracy of the current model. Rotating viscous flows in porous media were studied by Makinde et al. [24], while three-dimensional heat and mass transport in rotating nanofluids was studied by Sheikholeslami and Ganji [25]. Mustafa et al. [26], Archana et al. [27], and Sampath et al. [28] examined how Coriolis and Lorentz forces affect flow and heat transmission in rotating systems. Several other studies (Mabood et al. [29], Krishna and Chamkha [30], Kumar et al. [31] and Mustafa et al. [32]) have further explored rotational forces in fluid flow across a variety of physical scenarios. Moreover, the Coriolis force-arising from rotational effects-has been shown to influence flow direction and speed, especially in high-velocity or rotating systems, as discussed by several studies. However, a comprehensive study investigating the simultaneous influence of thermal radiation and Coriolis force on the flow of copper–alumina–water hybrid nanofluid over a rotating exponentially stretching surface is lacking in the literature. This research addresses that gap and aims to provide new insights relevant to both theoretical and applied sciences. Specifically, the study investigates the effects of increasing Coriolis force, magnetic field strength, inclination angle, and nanoparticle volume fraction on the skin friction, heat transfer rate, and overall behavior of the hybrid nanofluid flow.

In the pursuit of sustainable energy solutions, nanomaterials have emerged as key contributors due to their ability to enhance energy absorption and transfer efficiency. Among various renewable energy technologies, solar energy has gained prominence for its accessibility and environmental compatibility. Nanomaterials are well-suited to enhancing solar thermal systems due to their exceptional thermal diffusivity and large surface area, which enable them to absorb photons effectively. The importance of thermal radiation in enhancing heat transmission has been highlighted by recent research. Radioactive and magnetic field interactions in porous media were studied by Hayat et al. [33]. Radiative effects in nanofluid boundary layers were studied by Motsumi and Makinde [34] using the Runge-Kutta technique, and radiative MHD flow between rotating plates was studied by Sheikholeslami et al. [35]. Reddy et al. [36], Waqas et al. [37], Sreedevi et al. [38], and Gireesha et al. [40] demonstrate the growing interest in harnessing sun radiation to enhance fluid thermal performance.

The motivation for this study stems from the growing need for efficient heat transfer technologies in advanced engineering systems such as cooling of rotating machinery, electronic devices, solar collectors, and nuclear reactors. Although nanofluids have been extensively investigated, most existing works focus on limited physical effects, while a comprehensive analysis that simultaneously accounts for magnetic fields, rotation, nonlinear thermal radiation, viscous dissipation, Joule heating, and convective boundary conditions is remains limited. Therefore, the main objective of the present work is to analyze the three-dimensional magnetohydrodynamic flow and heat transfer of nanofluids under these combined influences. In addition, a comparative assessment of three different water-based nanofluids-copper, alumina, and ferrofluids-is carried out to highlight the distinct impact of nanoparticle type on the momentum and thermal fields, thereby providing useful insights into their relative performance for practical heat transfer applications.

Nomenclature

B_0	Applied magnetic field	T	Temperature
T_f	Surface temperature	q_r	radiative heat flux
C_p	Specific heat at constant pressure	h_f	heat transfer coefficient
k_{nf}	Thermal conductivity of nanofluid	u_w	Stretching velocity in x direction
u, v, w	The velocity components in the x,y,z directions(m/s)		

Greek words

Ω	Angular velocity	ϕ	The particle volume fraction parameter of the nanoparticle
μ	Dynamic viscosity of nanofluid	ρ	Density of nanofluid
σ^*	Stefan Boltzman constant	α	Thermal diffusivity of nanofluid
ρC_p	heat capacities	k^*	Mean absorption co-efficient

Subscripts

nf	nanofluid	s	solid nanoparticles
f	base fluid		

MATHEMATICAL FORMULATION

Here we discuss the numerical simulation of a three-dimensional, incompressible, electrically conducting nanofluid flow across a stretched surface that is convectively heated and exposed to magnetic and rotating forces. To investigate

changes in thermophysical behavior, Cu, Al_2O_3 and Fe_3O_4 nanoparticles are added to water, which serves as the working fluid. For any given value of a constant stretching rate, the surface extends along the x-axis at a velocity $u_w = ax$. Researchers like Reddy et al. [36], Waqas et al. [37], Sreedevi et al. [38], and Gireesha et al. [40] are interested in harnessing sun radiation to enhance fluid thermal performance. This work investigates how Coriolis and Lorentz forces collectively influence the steady three-dimensional boundary layer flow of nanofluids generated by a stretching surface.

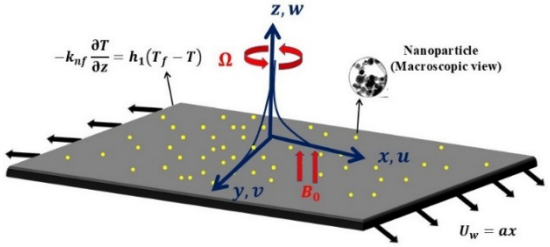

Figure 1. Geometry of the problem and coordinate system

Following the Tiwari-Das model's modifications for nanofluids and rotational effects, the flow is controlled by the continuity, momentum, and energy equations [41]. These equations are:

$$\frac{\partial u}{\partial x} + \frac{\partial v}{\partial y} + \frac{\partial w}{\partial z} = 0, \tag{2.1}$$

$$\rho_{nf}\left(u\frac{\partial u}{\partial x} + v\frac{\partial u}{\partial y} + w\frac{\partial u}{\partial z} - 2\Omega v\right) = \mu_{nf}\left(\frac{\partial^2 u}{\partial z^2}\right) - \sigma_{nf}B_0^2 u, \tag{2.2}$$

$$\rho_{nf}\left(u\frac{\partial v}{\partial x} + v\frac{\partial v}{\partial y} + w\frac{\partial v}{\partial z} + 2\Omega u\right) = \mu_{nf}\left(\frac{\partial^2 v}{\partial z^2}\right) - \sigma_{nf}B_0^2 v, \tag{2.3}$$

$$u\frac{\partial T}{\partial x} + v\frac{\partial T}{\partial y} + w\frac{\partial T}{\partial z} = \alpha_{nf}\left(\frac{\partial^2 T}{\partial z^2}\right) - \frac{1}{(\rho c_p)_{nf}}\frac{\partial q_r}{\partial z} + \frac{\mu_{nf}}{(\rho c_p)_{nf}}\left[\left(\frac{\partial u}{\partial z}\right)^2 + \left(\frac{\partial v}{\partial z}\right)^2\right] + \frac{\sigma_{nf}B_0^2}{(\rho c_p)_{nf}}[u^2 + v^2] + \frac{Q_T}{(\rho c_p)_{nf}}(T_f - T_\infty). \tag{2.4}$$

where q_r is the radiative heat flux modeled by the Rosseland approximation:

$$q_r = -\left(\frac{4\sigma^*}{3k^*}\right)\frac{\partial T^4}{\partial z}$$

The relevant boundary conditions for the present problem are;

$$u = u_w, \quad v = 0, \quad w = 0, \ -k_{nf}\frac{\partial T}{\partial z} = h_f(T_f - T) \ \ at\ z = 0,$$
$$u \to 0, \quad v \to 0, \quad T \to T_\infty \quad as \quad z \to \infty, \tag{2.5}$$

where u, v, and w represents the standard velocity components. x, y, and z directions respectively, while Ω is the fluid's constant angular velocity, ρ_{nf} -density of the nanofluid, μ_{nf} -dynamic viscosity of nanofluid, α_{nf} -thermal diffusivity of nanofluid, C_p-specific heat at constant pressure, B_0-applied magnetic field strength, h_f -heat transfer coefficient, k_{nf}-thermal conductivity of nanofluid, T -temperature, $q_r = -\left(\frac{4\sigma^*}{3k^*}\right)\frac{\partial T^4}{\partial z}$ is the Rosseland radiative heat flux and σ^* and k^* are the Stefan-Boltzman constant and the mean absorption coefficient.

NANOFLUID PROPERTIES

According to Brinkman [42], nanofluid viscosity is dynamic. μ_{nf} expressed as;

$$\mu_{nf} = \frac{\mu_f}{(1-\phi)^{2.5}}, \tag{2.6}$$

Effective density ρ_{nf} and effective heat capacity$(\rho c_p)_{nf}$ are expressed as [41];

$$\rho_{nf} = (1-\phi)\rho_f + \phi\rho_s, \tag{2.7}$$

$$(\rho c_p)_{nf} = (1-\phi)(\rho c_p)_f + \phi(\rho c_p)_s, \tag{2.8}$$

Below is the base fluid's thermal conductivity, and the Maxwell-Garnett model for nanofluid effective thermal conductivity is k_{nf}.

$$\frac{k_{nf}}{k_f} = \frac{(k_s+2k_f)-2\phi(k_f-k_s)}{(k_s+2k_f)+\phi(k_f-k_s)}, \tag{2.9}$$

moreover, the electrical conductivity of nanofluid σ_{nf} is given in the book by Maxwell [43] as;

$$\frac{\sigma_{nf}}{\sigma_f} = 1 + \frac{3(\sigma_s-\sigma_f)\phi}{(\sigma_s+2\sigma_f)-(\sigma_s-\sigma_f)\phi}, \tag{2.10}$$

where $(\rho C_p)_s$-volumetric heat capacity of solid nanoparticles, $(\rho C_p)_f$, $(\rho C_p)_{nf}$-are the base fluid's and the nanofluid's volumetric heat capacities, respectively., ϕ -a measure of nanoparticle volume fraction, ρ_f-density of base fluid, μ_f-dynamic viscosity of base fluid, k_s- the thermal conductivity of solid nanoparticles; the subscripts s and f indicate the solid and base fluids, respectively. Thermophysical parameters of water and nanoparticles are listed in Table 1.

Table 1. Thermophysical Characteristics of Base Fluid and Nanoparticles

	$\boldsymbol{\rho(kg/m^3)}$	$\boldsymbol{c_p(J/kgK)}$	$\boldsymbol{K(W/mk)}$	$\boldsymbol{\sigma(\Omega m)^{-1}}$
$\boldsymbol{Water}$	997.1	4179	0.613	0.05
$\boldsymbol{Fe_3O_4}$	5180	670	9.7	25000
Cu	8933	385	400	59.6
$\boldsymbol{Al_2O_3}$	3970	765	40	16.7

Equations (2.1), (2.2), (2.3) and (2.4), subject to the boundary conditions (2.5) admit similarity solutions in terms of the similarity functions f, g, θ and the similarity variable η and are defined as;

$$u = axf'(\eta), v = axg(\eta),$$
$$w = -\sqrt{\nu_f a} f(\eta), \theta(\eta) = \frac{T-T_\infty}{T_f-T_\infty}, \eta = \sqrt{\frac{a}{\nu_f}} z, \tag{2.11}$$

In view of the above quantities, the continuity Equation (2.1) is identically satisfied while Equations (2.2)–(2.5) become;

$$\frac{1}{(1-\phi)^{2.5}\left(1-\phi+\phi\frac{\rho_s}{\rho_f}\right)} f''' - f'^2 + ff'' + 2\lambda g - \frac{\sigma_{nf}/\sigma_f}{\left(1-\phi+\phi\frac{\rho_s}{\rho_f}\right)} Mf' = 0, \tag{2.12}$$

$$\frac{1}{(1-\phi)^{2.5}\left(1-\phi+\phi\frac{\rho_s}{\rho_f}\right)} g'' + fg' - f'g - 2\lambda f' - \frac{\sigma_{nf}/\sigma_f}{\left(1-\phi+\phi\frac{\rho_s}{\rho_f}\right)} Mg = 0, \tag{2.13}$$

$$\frac{1}{\left(1-\phi+\phi\frac{(\rho c_p)_s}{(\rho c_p)_f}\right)}\left[\frac{1}{Pr}\left(\left(\frac{K_{nf}}{k_f} + R(1+(\theta_w-1)\theta)^3\right)\theta'\right)'\right] + f\theta' +$$
$$\frac{1}{\left(1-\phi+\phi\frac{(\rho c_p)_s}{(\rho c_p)_f}\right)}\left\{\frac{1}{(1-\phi)^{2.5}} Ec(f''^2 + g'^2) + \frac{\sigma_{nf}}{\sigma_f} MEc(f'^2 + g^2)\right\} + \frac{Q_t\theta(\eta)}{\left(1-\phi+\phi\frac{(\rho c_p)_s}{(\rho c_p)_f}\right)} = 0 \tag{2.14}$$

The corresponding boundary conditions become;

$$f'(0) = 1,\ f(0) = 0,\ g(0) = 0\ \ \theta'(0) = Bi(\theta(0) - 1) \text{ at } \eta = 0,$$
$$f'(\eta) \to 0,\ g(\eta) \to 0,\ \theta(\eta) \to 0 \text{ as } \eta \longrightarrow \infty. \tag{2.15}$$

The magnetic parameter, radiation parameter, Prandtl number, heat source, Biot number, Eckert number, temperature ratio, and ratio of rotational rate to stretching rates are all examples of non-dimensional numbers.

$$M = \frac{\sigma_f {B_0}^2}{\rho_f a}, R = \frac{16\sigma^* T_\infty^3}{3k^* k_f}, Pr = \frac{(\mu c_p)_f}{k_f}, Q_t = \frac{Q_T}{\rho_f c_{pf}}, Bi = \frac{h_f}{k_{nf}}\sqrt{\frac{\nu_f}{a}}, Ec = \frac{u_w^2}{c_{pf}(T_f-T_\infty)}, \theta_w = \frac{T_f}{T_\infty}, \lambda = \frac{\Omega}{a}. \tag{2.16}$$

The quantities of practical interest are the skin friction coefficients C_{fx}, C_{fy} and the local Nusselt number N_{ux} defined as follows;

$$C_{fx} = \frac{\tau_{wx}}{\rho_f u_w^2},$$
$$C_{fy} = \frac{\tau_{wy}}{\rho_f u_w^2},$$
$$Nu_x = \frac{xq_w}{k_f(T_f-T_\infty)}, \tag{2.17}$$

where $\tau_{wx} = \tau_{zx}|_{z=0}$ and $\tau_{wy} = \tau_{zy}\big|_{z=0}$ are the wall shear stresses and q_w is the wall heat flux given by,

$$\tau_{wx} = \mu_{nf}\left.\frac{\partial u}{\partial z}\right|_{z=0},$$
$$\tau_{wy} = \mu_{nf}\left.\frac{\partial v}{\partial z}\right|_{z=0},$$

$$q_w = -k_{nf}\left.\frac{\partial T}{\partial z}\right|_{z=0} + q_r|_{z=0}. \tag{2.18}$$

Using equations (2.11) and (2.18) in equation (2.17), one obtains,

$$\sqrt{Re_x}\, C_{fx} = \frac{1}{(1-\phi)^{2.5}} f''(0),$$

$$\sqrt{Re_x}\, C_{fy} = \frac{1}{(1-\phi)^{2.5}} g'(0),$$

$$\frac{Nu_x}{\sqrt{Re_x}} = -\left(\frac{k_{nf}}{k_f} + R\theta_w^3\right)\theta'(0), \tag{2.19}$$

where $Re_x = \frac{u_w x}{\nu_f}$ is the local Reynolds number.

NUMERICAL METHOD

The reduced system of Eqs. (2.12) -(2.14), together with the boundary conditions (2.15), is solved numerically by employing the Runge-Kutta-Fehlberg fourth–fifth order (RKF45) scheme combined with the shooting technique. For this purpose, the coupled nonlinear ordinary differential equations are first converted into an equivalent system of first-order equations. This transformation enables the implementation of the shooting method, in which the unknown initial conditions are iteratively adjusted until the prescribed boundary conditions at infinity are satisfied to the desired accuracy.

Set $x_1 = f(\eta), x_2 = f'(\eta), x_3 = f''(\eta), x_4 = g(\eta), x_5 = \mathrm{g}'(\eta), x_6 = \theta(\eta), \mathrm{x}_7 = \theta'(\eta)$. Accordingly, we have;

$x_1' = x_2, x_2' = x_3, x_4' = x_5, x_6' = x_7,$

$$x_3{}' = (1-\phi)^{2.5}\left(1-\phi+\phi\frac{\rho_s}{\rho_f}\right)\left\{f'^2 + ff'' + 2\lambda g - \frac{\frac{\sigma_{nf}}{\sigma_f}}{\left(1-\phi+\phi\frac{\rho_s}{\rho_f}\right)}Mf'\right\}$$

$$x_5{}' = -(1-\phi)^{2.5}\left(1-\phi+\phi\frac{\rho_s}{\rho_f}\right)\left\{fg' - f'g - 2\lambda f' - \frac{\frac{\sigma_{nf}}{\sigma_f}}{\left(1-\phi+\phi\frac{\rho_s}{\rho_f}\right)}Mg\right\}$$

$$x_7{}' = -\frac{1}{\left(\frac{K_{nf}}{k_f} + R(1+(\theta_w-1)\theta)^3\right)}\left\{3R(1+(\theta_w-1)\theta)^2(\theta_w-1)\theta'^2 + \left(1-\phi+\phi\frac{(\rho c_p)_s}{(\rho c_p)_f}\right)Prf\theta' + Pr\left[\frac{1}{(1-\phi)^{2.5}}Ec(f''^2+g'^2) + \frac{\sigma_{nf}}{\sigma_f}MEc(f'^2+g^2) + Q_t\theta(\eta)\right]\right\}$$

$$x_1(0) = x_2(0) - 1 = x_3 - a_1 = x_4(0) = 0, x_5(0) - a_2 = x_6(0) - a_3 = x_7(0) - Bi(x_6(0) - 1) = 0. \tag{2.19}$$

here a_1, a_2 and a_3 are estimated via shooting technique. Afterwards, the resultant initial value problem is solved numerically via RK-Fehlberg method. The convergence criteria and step size are chosen as 10^{-6} and $\nabla\xi = 0.001$.

RESULTS AND DISCUSSION

The Runge-Kutta-Fehlberg (RKF45) method, in conjunction with a shooting method, is used numerically to solve the system of transformed nonlinear ordinary differential equations produced by similarity transformations. To ensure accuracy and stability of the solution, the convergence criterion is fixed at 10^{-6}, and a step size of $\Delta\eta = 0.001$ is used. The computational domain is truncated at a sufficiently large value of the similarity variable η, beyond which the boundary layer effects are negligible. The correctness of the numerical model is verified by comparing generated skin friction coefficients $f''(0)$ and $g'(0)$ for specific rotation parameter λ to benchmark findings in literature. [22, 23]. Table 2 shows the results of the comparison, which prove that the numerical system is reliable since there is high agreement.

Table 2. Comparison of Present Results with Existing Studies ($\phi = 0, M = 0$)

$\boldsymbol{\lambda}$	Wang [22]		Nazar et al. [23]		Present results	
	$f''(0)$	$\boldsymbol{g}'(0)$	$f''(0)$	$\boldsymbol{g}'(0)$	$f''(0)$	$\boldsymbol{g}'(0)$
0	-1	0	-1	0	-1.00006	0
0.5	-1.1384	-0.5128	-1.1384	-0.5128	-1.13837	-0.51276
1.0	-1.3250	-0.8371	-1.3250	-0.8371	-1.32503	-0.83710
2.0	-1.6523	-1.2873	-1.6523	-1.2873	-1.65235	-1.28726

Figures 2 and 3 demonstrate how the magnetic parameter M affects axial and transverse velocity profiles. As M increases, the axial velocity $f'(\eta)$ decreases due to the opposing Lorentz force, which acts as a resistive drag on the fluid motion. In contrast, the transverse velocity $g(\eta)$ shows an increasing trend with higher M, indicating enhanced secondary flow generated by the magnetic influence.

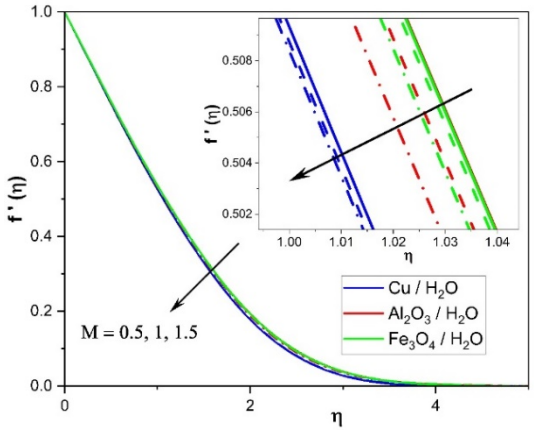

Figure 02. A study on the impact of a magnetic characteristic on speeds

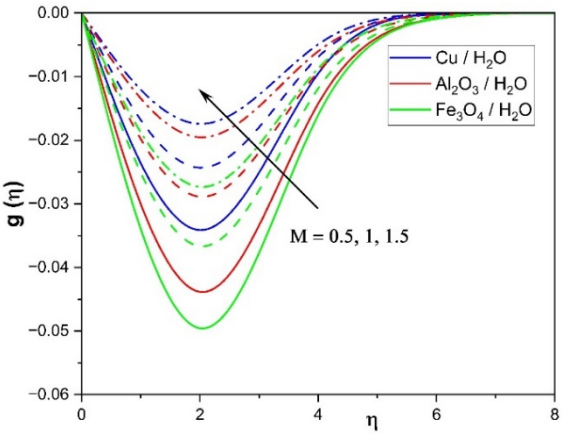

Figure 03. A study on the impact of a magnetic characteristic on speeds

In Figure 4, the temperature profile (η) increases with increasing M, mainly owing to ohmic heating effects from the magnetic field. Figures 5-7 illustrate how the rotation parameter λ affects the flow and heat fields. An increase in λ reduces the axial velocity while enhancing the transverse velocity, reflecting the rotational acceleration induced by the Coriolis force. The conversion of rotational energy into thermal energy causes a discernible increase in the temperature profile as λ values grow. This is because rotation introduces Coriolis acceleration, which diverts part of the momentum from the axial direction into the transverse direction. Consequently, energy is redistributed across velocity components, suppressing streamwise transport but enhancing lateral motion.

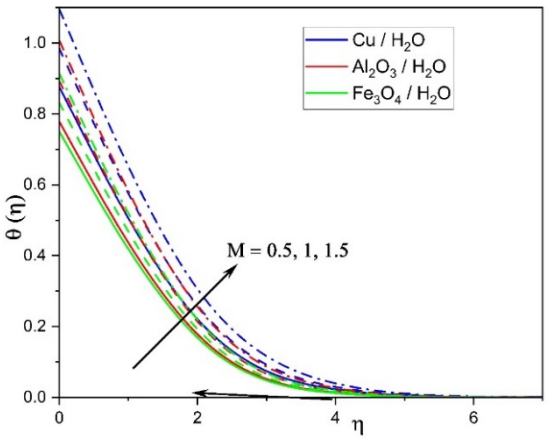

Figure 04. The impact of a magnetic parameter on a plot of temperatures

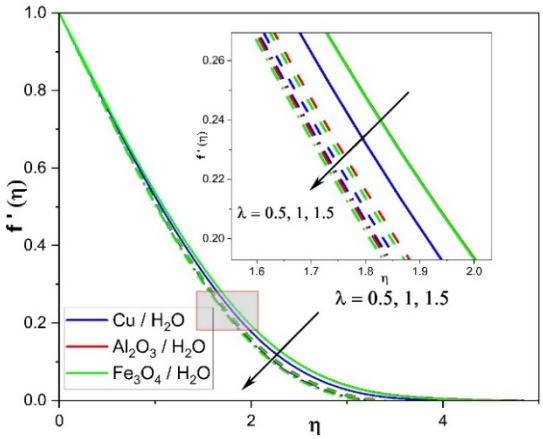

Figure 05. The velocity profile as a function of the stretching rate parameter and the ratio of the rotational speed to that parameter

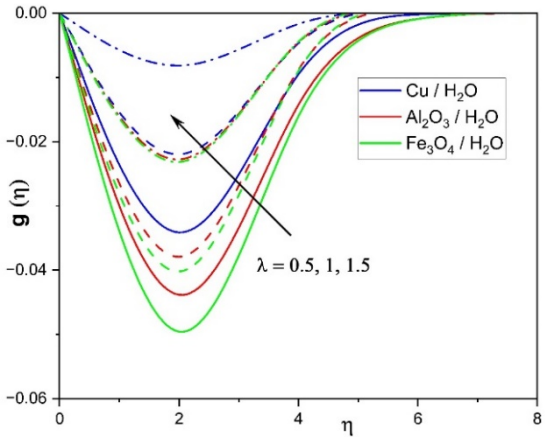

Figure 06. The impact on the velocity profile of the ratio of the stretching rate parameter to the rotation rate

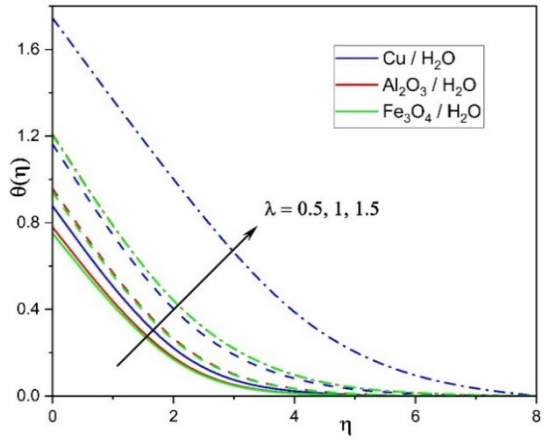

Figure 07. The influence of the ratio of rotation rate to the stretching rate parameter on the temperature profile

Figure 8 shows how the temperature distribution is affected by the nonlinear radiation parameter R. Nonlinear radiation augments energy transport by radiative diffusion, which enhances the effective thermal conductivity of the fluid,

thereby elevating the temperature profile. Figure 9 illustrates that increasing the temperature ratio parameter (θ_w) raises boundary layer temperatures and enhances thermal diffusion.

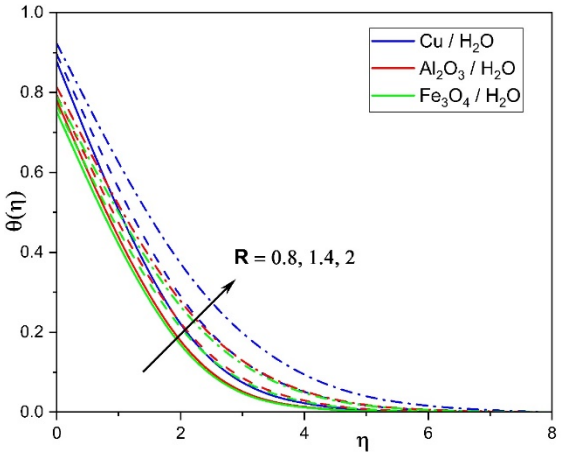

Figure 08. Heat profile as a function of radiation parameter

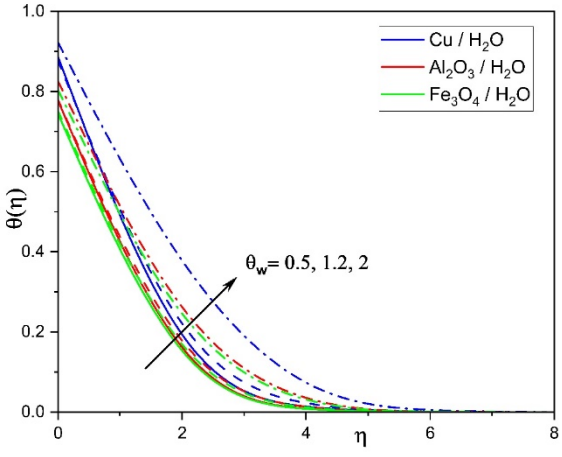

Figure 09. Changing the temperature profile according to a heat ratio parameter

In Figure 10, the Biot number (Bi), which characterizes the convective heat exchange at the surface, is varied. As Bi increases, the temperature near the surface increases due to a higher rate of convective heating, which promotes more efficient heat transfer into the fluid. A larger Bi corresponds to stronger thermal interaction between the solid boundary and the fluid. The influence of viscous dissipation is depicted in Figure 11 via the Eckert number (Ec). Ec values rise when internal fluid friction raises system temperature and thickens the thermal barrier layer, increasing thermal energy. Viscous dissipation converts mechanical work done by shear stresses into internal energy, while Joule heating transforms electromagnetic resistance into thermal energy. Both serve as internal heat generation mechanisms that elevate the fluid temperature.

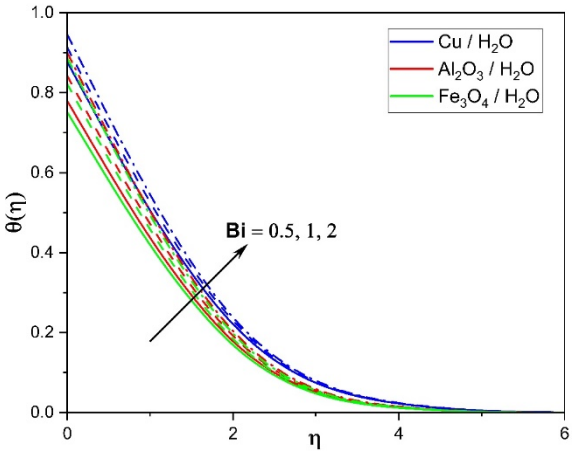

Figure 10. How the Biot number influences the temperature chart

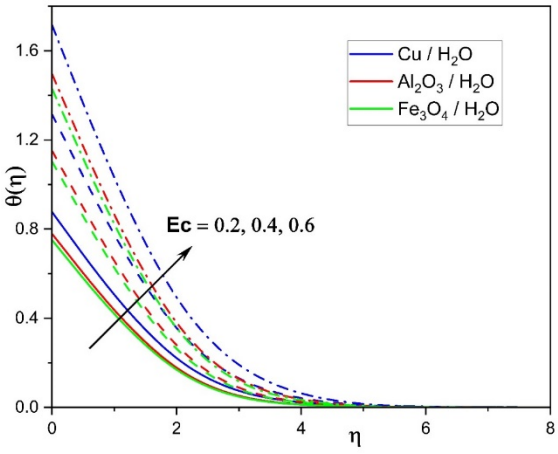

Figure 11. Understanding how the Eckert number influences the temperature profile

Figure 12 shows how the nanoparticle volume fraction ϕ affects the temperature field. Due to the nanofluid's enhanced thermal conductivity and heat absorption capability, the temperature distribution becomes more noticeable as ϕ grows. This increases thermal diffusion because the fluid can retain more heat. Figure 13 illustrates the effect of the internal heat source parameter. As Qt increases, the temperature within the boundary layer rises substantially, indicating a direct enhancement in internal energy generation which results in a thicker thermal boundary layer and stronger temperature in fluids. With regard to the parameters λ and M, Figures 14 and 15 show the fluctuation of the skin friction coefficients in x and y directions. It is observed that increasing λ and M leads to a reduction in axial skin friction, indicating a decrease in surface shear stress. However, C_{fy} increases with M due to enhanced resistance in the transverse direction caused by the Lorentz force, while it decreases with λ, as rotational motion reduces transverse shear. Figure 16 shows the variation of the local Nusselt number with respect to λ and M. Nusselt number decreases when either parameter rises, suggesting wall convective heat transmission decreases. The dampening effect of magnetic and rotating forces decreases the thickness of thermal boundary layer. Figure 17 demonstrates how Eckert number and nanoparticle concentration effect Nusselt number. A synergistic impact between thermal energy production and increased thermal

conductivity owing to nanoparticles is shown by the fact that raising either parameter boosts the heat transfer rate. Among the nanofluids considered, the Cu-based fluid consistently shows the highest heat transfer performance, followed by Al_2O_3 and Fe_3O_4, respectively. These results underscore the significance of controlling magnetic, rotational, and thermal parameters to optimize heat and momentum transport in nanofluid-based systems. They also reinforce the crucial role of nanoparticle material selection in designing efficient thermal management technologies.

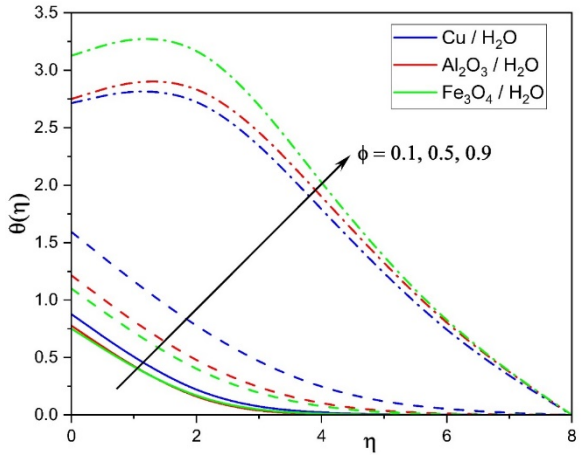

Figure 12. How the parameter for solid volume fraction affects the temperature profile

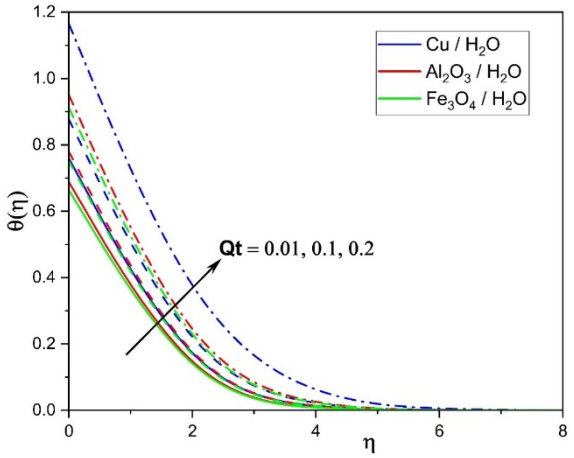

Figure 13. Heat source parameter influence on temperature profile

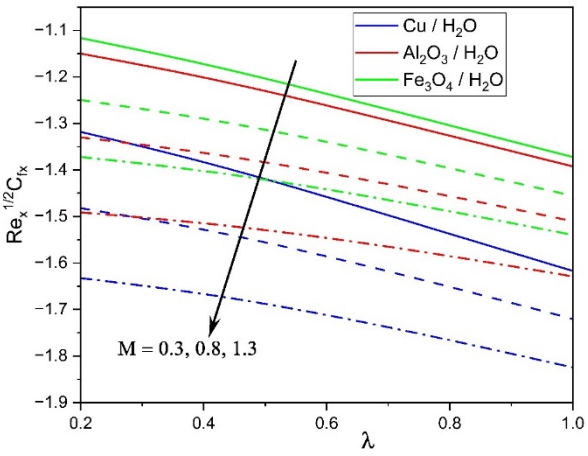

Figure 14. A study on the skin friction coefficient and its relationship to the magnetic parameter, rotation rate, and stretching rate

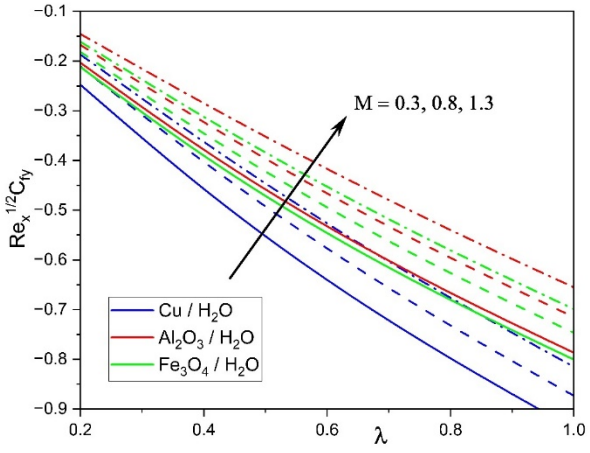

Figure 15. A study on the skin friction coefficient and its relationship to the magnetic parameter, rotation rate, and stretching rate

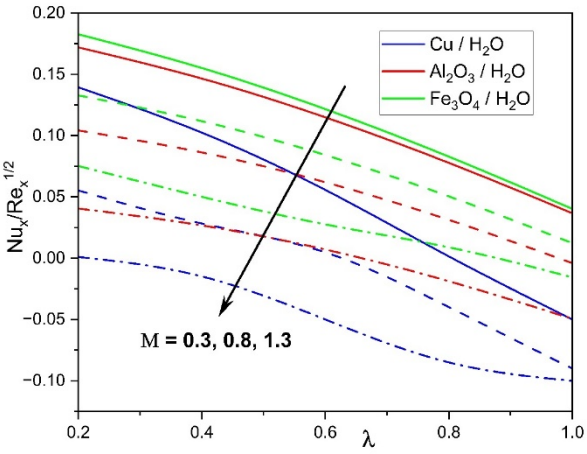

Figure 16. The skin friction coefficient as a function of the magnetic parameter and the ratio of the rotational speed to the stretching rate

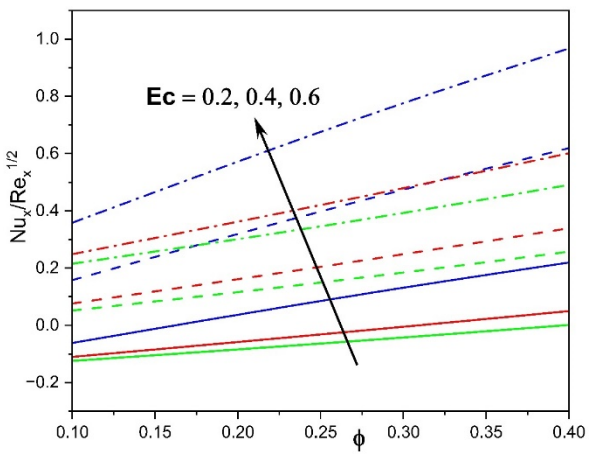

Figure 17. Nusselt number impacted by Eckert number v/s ϕ

Table 3 highlights the influence of nanoparticle concentration (ϕ), radiation parameter (R), Biot number (Bi), and Eckert number (Ec) on skin-friction coefficients and heat transfer for Fe_3O_4, Al_2O_3, and Cu nanofluids.

Table 3. Variation of $Re_x^{0.5}C_{fx}$, $Re_x^{0.5}C_{fy}$ and $Re_x^{-0.5}Nu$ for Fe_3O_4, Al_2O_3 and cu nanofluids with different values of ϕ, R, Bi and Ec

ϕ	R	Bi	Ec	Fe_3O_4			Al_2O_3			cu		
				$\sqrt{Re_x}\,C_{fx}$	$\sqrt{Re_x}\,C_{fy}$	$\frac{Nu_x}{\sqrt{Re_x}}$	$\sqrt{Re_x}\,C_{fx}$	$\sqrt{Re_x}\,C_{fy}$	$\frac{Nu_x}{\sqrt{Re_x}}$	$\sqrt{Re_x}\,C_{fx}$	$\sqrt{Re_x}\,C_{fy}$	$\frac{Nu_x}{\sqrt{Re_x}}$
0.1				-2.57614	-1.12919	-0.1471	-2.51119	-1.0574	0.11598	-2.76735	-1.3362	-0.70944
0.4				-6.11419	-2.46404	0.762076	-5.81055	-2.11379	1.552431	-6.96659	-3.40968	-0.65158
0.8				-42.1525	-8.8709	-5.71607	-40.4565	-7.15531	-5.22018	-45.3067	-14.118	-5.20013
	1			-2.57614	-1.12919	-0.1471	-2.51119	-1.0574	0.11598	-2.76735	-1.3362	-0.70944
	2			-2.57614	-1.12919	0.12487	-2.51119	-1.0574	0.313545	-2.76735	-1.3362	-0.30353
	3			-2.57614	-1.12919	0.828804	-2.51119	-1.0574	1.04208	-2.76735	-1.3362	0.370026
		0.4		-2.57614	-1.12919	-0.1471	-2.51119	-1.0574	0.11598	-2.76735	-1.3362	-0.70944
		0.8		-2.57614	-1.12919	-0.22649	-2.51119	-1.0574	0.189343	-2.76735	-1.3362	-0.99507
		1.5		-2.57614	-1.12919	-0.30282	-2.51119	-1.0574	0.269242	-2.76735	-1.3362	-1.23501
			0.2	-2.57614	-1.12919	-0.1471	-2.51119	-1.0574	0.11598	-2.76735	-1.3362	-0.70944
			0.5	-2.57614	-1.12919	-0.74056	-2.51119	-1.0574	-0.00332	-2.76735	-1.3362	-1.76428
			0.7	-2.57614	-1.12919	-0.62222	-2.51119	-1.0574	-0.08866	-2.76735	-1.3362	-2.27411

Increasing ϕ enhances both axial and transverse skin friction due to higher viscosity, with Cu showing the highest resistance, while the Nusselt number generally decreases, except for Al_2O_3 which sustains better heat transfer. Larger R values intensify transverse skin friction through stronger Coriolis forces but improve heat transfer, where Al_2O_3 performs best. Variation in Bi reveals that Al_2O_3 nanofluid enhances convective heat exchange, whereas Fe_3O_4 and Cu exhibit reduced Nusselt numbers. The Eckert number increases internal heating and suppresses cooling for $Fe_3O_4$and Cu, while Al_2O_3 shows a mild positive response due to its superior thermal conductivity. Overall, Cu exhibits strong flow resistance, Fe_3O_4 provides stability, and Al_2O_3 consistently demonstrates the best heat transfer characteristics, making it the most efficient choice under varying conditions.

CONCLUSIONS

This study provides new physical insights into the three-dimensional MHD nanofluid flow over a stretching surface under the combined influences of rotation, magnetic field, nonlinear radiation, Joule heating, and viscous dissipation. From a physics standpoint, the following key conclusions can be drawn:

- Rotation fundamentally redistributes momentum between the axial and transverse directions. While axial motion is suppressed, transverse velocity is enhanced, indicating that rotational energy is redirected into lateral flow, which modifies transport mechanisms across the boundary layer.
- The applied magnetic field resists fluid motion, thickening the momentum boundary layer, while simultaneously enhancing heat generation through Ohmic dissipation. This coupling shows how electromagnetic control can tune both fluid resistance and energy transport.
- Nonlinear radiation, internal heat generation, and convective surface effects act collectively to strengthen energy diffusion across the boundary layer. Their combined impact illustrates the importance of radiative and convective modes in enhancing nanoscale thermal transport.
- Viscous and Joule dissipation provide an internal energy feedback mechanism, where mechanical work against friction and electromagnetic resistance is directly converted into heat, raising the fluid temperature and altering thermal boundary layer dynamics.
- The comparative analysis of Cu, Al_2O_3, and Fe_3O_4 nanofluids demonstrates that nanoparticle type is a decisive factor in tuning flow and heat transfer. Cu-water nanofluid exhibits the strongest heat transfer enhancement due to its high thermal conductivity, whereas Fe_3O_4-water shows superior flow adaptability under magnetic control, making it advantageous for MHD applications.

Acknowledgements: The author would like to thank GITAM Deemed to be University for providing the MATLAB Software.

Funding: There is no funding received by any agency.

Data Availability Statement: This article contains all the pertinent data generated or analysed during this investigation; further material can be provided upon reasonable request to the authors.

Declaration: We, the authors of this manuscript, declare that this work is original and has not been published or submitted elsewhere for consideration.

Conflict of Interest: The author declares that there is no conflict of interest

ORCID

M.M. Bindu, https://orcid.org/0009-0001-6250-8606; **Elliriki Mamatha,** https://orcid.org/0000-0002-1512-5063
V. Nagaradhika, https://orcid.org/0000-0002-0927-7191

REFERENCE

[1] S.U.Choi, and J.A. Eastman, *Enhancing thermal conductivity of fluids with nanoparticles* (No. ANL/MSD/CP-84938; CONF-951135-29), (Argonne National Lab. (ANL), Argonne, IL, United States), (1995).
[2] J. Buongiorno, "Convective transport in nanofluids," ASME J. Heat Transf., **128**, 240–250 (2006). https://doi.org/10.1115/1.2150834
[3] Wang, Xiaoming, Changhe Li, Yanbin Zhang, Wenfeng Ding, Min Yang, Teng Gao, Huajun Cao, *et al*. "Vegetable oil-based nanofluid minimum quantity lubrication turning: Academic review and perspectives," Journal of Manufacturing Processes, **59**, 76-97 (2020). https://doi.org/10.1016/j.jmapro.2020.09.044
[4] M. Sheikholeslami, and H.B. Rokni, "Nanofluid two phase model analysis in existence of induced magnetic field," International Journal of Heat and Mass Transfer, **107**, 288-299 (2017). https://doi.org/10.1016/j.ijheatmasstransfer.2016.10.130
[5] W.A. Khan, and I. Pop, "Boundary-layer flow of a nanofluid past a stretching sheet," International journal of heat and mass transfer, **53**(11-12), 2477-2483 (2010). https://doi.org/10.1016/j.ijheatmasstransfer.2010.01.032
[6] M.R. Krishnamurthy, B.J. Gireesha, R.S.R. Gorla, and B.C. Prasannakumara, "Suspended particle effect on slip flow and melting heat transfer of nanofluid over a stretching sheet embedded in a porous medium in the presence of nonlinear thermal radiation," Journal of Nanofluids, **5**(4), 502-510(2016). https://doi.org/10.1166/jon.2016.1247
[7] N. Muqaddass, F. Mabood, S.A. Shehzad, F. Sahar, and I.A. Badruddin, "Analysis of heat transportation in a convectively heated time-dependent $CuAl_2O_3$-H_2O hybrid nanofluid with varying thermal conductivity," Proceedings of the Institution of Mechanical Engineers, Part C: Journal of Mechanical Engineering Science, **238**(6), 2513-2520 (2024). https://doi.org/10.1177/09544062231187788
[8] S. Nadeem, N. Abbas, and M.Y. Malik, "Inspection of hybrid based nanofluid flow over a curved surface," Computer methods and programs in biomedicine, **189**, 105193 (2020). https://doi.org/10.1016/j.cmpb.2019.105193
[9] A. Asadi, I.M. Alarifi, and L.K. Foong, "An experimental study on characterization, stability and dynamic viscosity of CuO-TiO2/water hybrid nanofluid," Journal of Molecular Liquids, **307**, 112987 (2020). https://doi.org/10.1016/j.molliq.2020.112987
[10] K. Das, P.R. Duari, and P.K. Kundu, "Nanofluid flow over an unsteady stretching surface in presence of thermal radiation," Alex. Eng. J. **53**(3), 737–745 (2014). https://doi.org/10.1016/j.aej.2014.05.002
[11] L. Roohi, "Nanofluid flow in a converging and diverging channel of rectangular and heated walls," Ain Shams Engineering Journal, **12**(4), 4023-4035 (2021). https://doi.org/10.1016/j.asej.2021.02.030
[12] K. Ur Rehman, M.Y. Malik, O.D. Makinde, and A.A. Malik, "A comparative study of nanofluids flow yields by an inclined cylindrical surface in a double stratified medium," The European Physical Journal Plus, **132**(10), 427 (2017). https://doi.org/10.1140/epjp/i2017-11679-1
[13] O.D. Makinde. "Computational modelling of nanofluids flow over a convectively heated unsteady stretching sheet," Current Nanoscience, **9**(5), 673-678 (2013). https://doi.org/10.2174/15734137113099990068
[14] N.S. Akbar, M.F. Hussain, M. Alghamdi, and T. Muhammad, "Thermal characteristics of magnetized hybrid Casson nanofluid flow in a converging–diverging channel with radiative heat transfer: A computational analysis," Scientific Reports, **13**(1), 21891 (2023). https://doi.org/10.1038/s41598-023-49397-3
[15] U. Khan, I. Waini, A. Zaib, A. Ishak, and I. Pop, "MHD mixed convection hybrid nanofluids flow over a permeable moving inclined flat plate in the presence of thermophoretic and radiative heat flux effects," Mathematics, **10**(7), 1164 (2022). https://doi.org/10.3390/math10071164
[16] B.J. Gireesha, and L. Anitha, "Convective flow of couple stress ternary nanoliquid flow through a permeable microchannel: irreversibility analysis," International Journal of Modelling and Simulation, 1-18 (2024). https://doi.org/10.1080/02286203.2024.2388117
[17] J.K. Madhukesh, G.K. Ramesh, H.N. Fatima, G.S. Roopa, and S.A. Shehzad, "Influence of pollutant dispersion on nanofluid flowing across a stretched disc-cone device," Journal of Molecular Liquids, **411**, 125710 (2024). https://doi.org/10.1016/j.molliq.2024.125710
[18] W. Cheng, M. Safeer, U. Farooq, S. Munir, J. Cui, and C.S.K. Raju, "Nonsimilar forced convection simulations of water-copper nanofluid flow through a porous medium in the presence of thermal radiations, heat generation and viscous dissipation," Waves in Random and Complex Media, **35**(1), 511-526 (2025). https://doi.org/10.1080/17455030.2021.2023785
[19] M. Sheikholeslami, and S.A. Shehzad, "Magnetohydrodynamic nanofluid convection in a porous enclosure considering heat flux boundary condition," International Journal of Heat and Mass Transfer, **106**, 1261-1269 (2017). https://doi.org/10.1016/j.ijheatmasstransfer.2016.10.107
[20] D.K. Jyoti, V. Nagaradhika, P.B.S. Kumar, and A.J. Chamkha, "Nonlinear Convection and Radiative Heat Transfer in Kerosene-Alumina Nanofluid Flow Between Two Parallel Plates with Variable Viscosity," Journal of Nanofluids, **13**(5), 1055-1062 (2024). https://doi.org/10.1166/jon.2024.2193
[21] T.V. Karman, "Über laminar and turbulent Reibung," ZAMM, J. App. Math. Mech. **1**(4), 233–252 (1921).
[22] C.Y. Wang, "Stretching a surface in a rotating fluid", ZAMP, **39**(2), 177–185 (1988). https://doi.org/10.1007/BF00945764
[23] R. Nazar, N. Amin, and I. Pop, "Unsteady boundary layer flow due to a stretching surface in a rotating fluid," Mech. Res. Commun. **31**(1), 121–128 (2004). https://doi.org/10.1016/j.mechrescom.2003.09.004
[24] O.D. Makinde, O.A. Bég, and H.S. Takhar, "Magnetohydrodynamic viscous flow in a rotating porous medium cylindrical annulus with an applied radial magnetic field," Int. J. Appl. Math. Mech. **5**(6), 68-81 (2009).
[25] M. Sheikholeslami, and D.D. Ganji, "Three-dimensional heat and mass transfer in a rotating system using nanofluid," Powder Technol. **253**, 789–796 (2014). https://doi.org/10.1016/j.powtec.2013.12.042
[26] M. Mustafa, A. Mushtaq, T. Hayat, and A. Alsaedi, "Rotating flow of magnetite-water nanofluid over a stretching surface inspired by non-linear thermal radiation," PloS one, **11**(2), e0149304 (2016). https://doi.org/10.1371/journal.pone.0149304
[27] M. Archana, B.J. Gireesha, B.C. Prasannara, and R.S.R. Gorla, "Influence of nonlinear thermal radiation on rotating flow of Casson nanofluid, Nonlinear Engineering, **7**(2), 91-101 (2017). https://doi.org/10.1515/nleng-2017-0041
[28] P.B. Sampath Kumar, B.J. Gireesha, B. Mahanthesh, and R.S.R. Gorla, "Radiative nonlinear 3D flow of ferrofluid with Joule heating, convective condition and Coriolis force," Thermal Science and Engineering Progress, **3**, 88-94 (2017). https://doi.org/10.1016/j.tsep.2017.06.006

[29] F. Mabood, W.A. Khan, and O.D. Makinde, "Hydromagnetic flow of a variable viscosity nanofluid in a rotating permeable channel with Hall effects," Journal of Engineering Thermophysics, **26**(4), 553-566 (2017). https://doi.org/10.1134/S1810232817040105
[30] M.V. Krishna, and A,J. Chamkha, "Hall and ion slip effects on MHD rotating boundary layer flow of nanofluid past an infinite vertical plate embedded in a porous medium," Results in Physics, **15**, 102652 (2019). https://doi.org/10.1016/j.rinp.2019.102652
[31] S.S. Kumar, RV Prasad, S.U. Mamatha, C.S.K. Raju, and B.M. Rao, Dynamics of nonlinear-shaped solid particles occurrence of hydro-magnetic slip with comparative analysis of radiated ternary, hybrid and nanofluid flow in a rotating internally, International Journal of Modern Physics B, **37**(13), 2350127 (2023). https://doi.org/10.1142/S0217979223501278
[32] Z. Mustafa, T. Hayat, T. Javed, and A. Alsaedi, "Unsteady MHD Casson fluid flow with Dufour and Soret's effects due to a rotating cone," Waves in Random and Complex Media, (2023). https://doi.org/10.1080/17455030.2023.2188099
[33] T. Hayat, Z. Abbas, I. Pop, and S. Asghar, "Effects of radiation and magnetic field on the mixed convection stagnation-point flow over a vertical stretching sheet in a porous medium," International Journal of Heat and Mass Transfer, **53**(1-3), 466-474 (2010). https://doi.org/10.1016/j.ijheatmasstransfer.2009.09.010
[34] T.G. Motsumi, and O.D. Makinde, "Effects of thermal radiation and viscous dissipation on boundary layer flow of nanofluids over a permeable moving flat plate," Physica Scripta, **86**(4), 045003 (2012). https://doi.org/10.1088/0031-8949/86/04/045003
[35] M. Sheikholeslami, T. Hayat, and A. Alsaedi, "MHD free convection of Al2O3-water nanofluid considering thermal radiation: a numerical study," International Journal of Heat and Mass Transfer, **96**, 513-524 (2016). https://doi.org/10.1016/j.ijheatmasstransfer.2016.01.059
[36] S.J. Reddy, P. Valsamy, and D.S. Reddy, "Thermal Radiation Impact on Nanofluid Boundary Layer Flow Towards a Moving Plate in Presence of Magnetic Field Using Numerical Solutions," Journal of Nanofluids, **13**(1), 199-206 (2024). https://doi.org/10.1166/jon.2024.2144
[37] W. Hassan, U. Farooq, D. Liu, M. Abid, M. Imran, and T. Muhammad, "Heat transfer analysis of hybrid nanofluid flow with thermal radiation through a stretching sheet: A comparative study," International Communications in Heat and Mass Transfer, **138**, 106303 (2022). https://doi.org/10.1016/j.icheatmasstransfer.2022.106303
[38] P. Sreedevi, P.S. Reddy, and A. Chamkha, "Heat and mass transfer analysis of unsteady hybrid nanofluid flow over a stretching sheet with thermal radiation," SN Applied Sciences, **2**(7), 1222 (2020). https://doi.org/10.1007/s42452-020-3011-x
[39] R. Devi, S.V. Venkata, and M.G. Reddy, "Parametric analysis of MHD flow of nanofluid in stretching sheet under chemical sensitivity and thermal radiation," Heat Transfer, **51**(1), 948-975 (2022). https://doi.org/10.1002/htj.22337
[40] B.J. Gireesha, G. Sowmya, M.I. Khan, and H.F. Öztop, "Flow of hybrid nanofluid across a permeable longitudinal moving fin along with thermal radiation and natural convection," Computer methods and programs in biomedicine, **185**, 105166 (2020). https://doi.org/10.1016/j.cmpb.2019.105166
[41] R.K. Tiwari, and M.K. Das, "Heat transfer augmentation in a two-sided lid-driven differentially heated square cavity utilizing nanofluids," Int. J. Heat Mass Transf. **50**, 2002–2018 (2007). https://doi.org/10.1016/j.ijheatmasstransfer.2006.09.034
[42] H.C. Brinkman, "The viscosity of concentrated suspensions and solutions," J. Chem. Phys. **20**, 571–581 (1952). https://doi.org/10.1063/1.1700493
[43] J.C. Maxwell, *A treatise on electricity and magnetism*, Second Ed., (Cambridge, Oxford University Press, 1904). pp. 435-441.

ТРИВИМІРНИЙ МГД-ПОТІК ТА ТЕПЛОПЕРЕНОС НАНОРІДИН НА ВОДНІЙ ОСНОВІ ЧЕРЕЗ ПОВЕРХНЮ ЩО РОЗТЯГУЄТЬСЯ ЗА ДОПОМОГОЮ СИЛИ КОРІОЛІСА ТА ТЕПЛОВИХ ЕФЕКТІВ

М.М. Бінду[1,2], Еллірікі Маматха[2], В. Нагарадхіка[3]

[1]Державний коледж першого ступеня, Чаннапатна, 562160, Індія
[2]Кафедра математики, GSS, GITAM Deemed to be University, Бенгалур-561203, Індія
[3]Кафедра математики, Технологічний інститут сера М. Вісвесвараї, Бенгалур-562 157, Індія

Це дослідження зосереджено на тепловій поведінці та тривимірному пограничному шарі потоку нанорідин на водній основі на розтягнутій поверхні з урахуванням комбінованого впливу сил Коріоліса та Лоренца. Модель включає кілька важливих фізичних аспектів, таких як поверхнева конвекція, внутрішнє теплоутворення, джоулеве нагрівання, в'язка дисипація та теплове випромінювання. Наночастинки міді (Cu), оксиду алюмінію (Al_2O_3) та магнетиту (Fe_3O_4) диспергуються у воді для порівняння їхньої ефективності у посиленні теплопередачі. Застосовуючи перетворення подібності, складна система диференціальних рівнянь з частинними похідними зводиться до набору нелінійних звичайних диференціальних рівнянь, які потім розв'язуються чисельно за допомогою методу Рунге-Кутти-Фельберга разом з методом стрільби. Результати показують, що нанорідини, що містять наночастинки Cu, забезпечують найвищі теплові характеристики, далі йдуть ті, що містять Al_2O_3 та Fe_3O_4. Ці результати підкреслюють важливість вибору відповідних наночастинок для покращення ефективності теплопередачі в застосуваннях для терморегуляції. Збільшення параметра обертання λ пригнічує осьову швидкість, одночасно зменшуючи розподіл температури, підкреслюючи вплив демпфування обертальних ефектів на імпульс та теплоперенос.

Ключові слова: *нелінійне теплове випромінювання; нанорідина; обертальні ефекти; в'язка дисипація; джоулевий нагрів*